Romanian Reports in Physics, Vol. 66, No. 2, P. 455–471, 2014

K-SHELL IONIZATION CROSS SECTIONS OF Ti, Cr, Ni, Cu, AND Zr IN COLLISIONS WITH ^{16}O IONS AT MeV/u ENERGIES

A.C. SCAFES[1*], C. CIORTEA[1], D.E. DUMITRIU[1], A. ENULESCU[1], D. FLUERASU[1], M.M. GUGIU[1], M.D. PENA[1], M. PENTIA[1], AND I. PITICU[1]

[1]"Horia Hulubei" National Institute for Physics and Nuclear Engineering (IFIN-HH), P.O.Box MG-6 Măgurele, 077125 Bucharest, Romania, [*]E-mail: ascafes@tandem.nipne.ro

Received March 14, 2013

Abstract. Using the 9 MV Van de Graaff Tandem accelerator of IFIN-HH, integral shell ionization cross sections of Ti, Cr, Ni, Cu and Zr by ^{16}O ions in the energy range of 0,5–3 MeV/u have been determined. By the energy and yield shifts method, outer-shell multiple ionization is analyzed. L- and M-shell multiple ionization probabilities per electron are estimated and compared with the geometrical model predictions. The experimental cross sections are compared with calculations using the semi-classical approximation (SCA), in the united atom (UA) and separated atom (SA) limits, as well as the ECPSSR model calculations. The ECPSSR calculations are in close proximity to data, although slightly higher.

Key words: K X-ray yields, K-shell ionization cross-sections, outer-shell multiple ionization.

1. INTRODUCTION

An accurate knowledge of data of integral cross sections induced by energetic ions is of interest both for applications and as a testing ground for theoretical formulations of ion-atom collision mechanisms and inner-shell ionization processes. In the present paper we report K-shell ionization cross-sections for energetic oxygen ion beams in the MeV/u energy range bombarding different thin solid targets. Ionization cross sections are necessary e.g. in elemental analysis by the particle-induced X-ray emission (PIXE) method (see ref. [1] and examples in refs. [2, 3]) with energetic ions heavier than protons [4].

PIXE is an analytical method with high sensitivity (in the ppm range) for many elements when thin sample targets are analyzed, i.e. targets for which the energy loss (ΔE) is negligible compared to incident energy (E_0, of several MeV/u energy), therefore $\Delta E/E_0 << 1$. For thick samples (see e.g. [5]), which are easier to prepare, the sensitivity is lower, but the PIXE method can be applied for determining the composition of major elements. The facts that the PIXE method

can be standardized, allows fast and accurate analysis of more elements simultaneously. This can be applied to small amounts of sample made it widely applied in laboratories where a small charged particle accelerator is available, often coupled with other ion beam analysis (IBA) methods to obtain analytical data in various fields of environmental, biological, medical, archaeological etc. interest.

The sensitivity of the PIXE method depends on, both, the X-ray production and background yields. In the case of very asymmetric collision with light ion beams (protons, mostly used in PIXE [6, 7], alphas etc.), the ionization cross sections are well described by ionization models in the first order perturbation theory, as plane wave Born approximation (PWBA) [8] and semi-classical approximation (SCA) [9]. At MeV/u collision energies, the ionization cross sections data show a strong dependence on the binding energy of the active electron in the initial state. For unmodified binding, the models in the first order of perturbation theory predict a dependence on the square of the atomic number (Z_1) of the projectile. A good quantitative description of the experimental data for light ions at energies of the order of MeV/u was obtained from the ECPSSR model calculations [10,11], which using PWBA as starting point take into account effects like increased binding energy and relativistic motion of the electron, deflection of the projectile etc.

In some applications of the PIXE method, it is necessary to increase the X-ray yield for medium- and high-Z elements without excessive increasing of the beam intensity. This can be achieved by increasing the ion beam energy, with the expense of higher background intensity. Another method that can be applied in these cases is the use of heavier ion beams, having an atomic number $Z_1 > 1$, due to the (approximate) dependence on Z_1^2 of the ionization cross sections at equal velocities.

During the energetic ions collisions, the strong Coulomb field of the projectile nucleus can cause simultaneously ejection of one or more outer-shell electrons besides the K-shell electron. This multiple ionization increases the binding energy of the remaining electrons and modifies the transition probabilities. Instead of a single-vacancy X-ray transition (diagram line), more X-ray transitions (satellites) are produced. The satellite structure cannot be resolved with a low-resolution X-ray spectrometer like that using a semiconductor detector. In this case, the multiple ionization results in energy shift and enlarged X-ray lines as well as in relative intensity modifications. The procedure of measuring the X-ray energy and yield shifts was introduced to obtain information on the outer-shell multiple ionization effect (see e.g. ref. [12]).

Measurements of K-shell ionization cross sections for intermediate-Z elements by ^{16}O ions at energies in the MeV/u range have been reported before (see e.g. ref. [4, 13–19]). Still, the data useful in the literature for PIXE applications are rather limited, therefore in the present paper determination of integral K-shell

ionization cross sections by MeV/u energy ^{16}O ion beams was proposed. K-shell ionization cross sections obtained from measurements of K X-ray yields of Ti, Cr, Ni, Cu and Zr thin solid targets are reported.

An analysis of the multiple ionization of the outer (L, M) shells during K-shell ionization, by measuring the energy and yield shifts of the K X-rays, was also done. The energy and yield shifts method was applied to estimate mean numbers of the outer-shell spectator vacancies as well as correction factors to the fluorescence yields due to multiple ionization effects.

Further, in the present paper, the multiple ionization effect is treated in some detail (section 2) and is followed by presentation of experimental procedure (section 3), results and discussion (section 4).

2. MULTIPLE IONIZATION

In processes like photo-ionization, radioactive decay (by electron capture or internal conversion), bombardment with electrons and protons, K or L X-ray spectra well described as due to only one internal (K-, L-) vacancy are produced. However, detailed studies of small energy shifts of X-ray lines (see e.g. ref. [20]) showed that, even in these cases, outer-shell multiple ionization plays a role. Instead, bombarding a target atom with heavier energetic ions results in a strong disturbance due to Coulomb interaction, so in addition to inner-shell (K, L) vacancies, production of additional outer-shell vacancies is a rule, rather an exception. Under these conditions, energy and yield shifts [12] are more easily measured and, using high resolution crystal spectrometers, satellite lines can be solved [21, 22]. Thus, KL^n satellite lines due to n spectator vacancies in the L-shell during K-vacancy decay were observed and studied [23, 24]. As a general characteristic, the intensities of these satellites can be understood qualitatively on the basis of a first order semi-classical approximation [25], which gives an ionization cross section $\sigma \sim Z_1^2/Z_2^4$, where Z_1, Z_2 are the atomic numbers of the projectile and target, respectively. In addition, assuming the excitation of an electron is not influenced by the interaction with others (the independent electron approximation) [26] leads to a statistical binomial distribution for producing multiple vacancies. A perturbation theory approximation in the first order is expected to be an adequate description in the cases where the production probability of multiple vacancies is not too high. For a very strong perturbation, which results in the emission of an important part of the shell electrons, a more appropriate description by a non-perturbation model like the geometric model [27] could be done.

In an independent electron approximation (IEA), the probability to ionize q_i electrons out of N_i electrons, the occupancy number of the Y_i shell (subshell), is given by the binomial distribution:

$$P_{q_i} = C_{N_i}^{q_i} p_i^{q_i} (1-p_i)^{N_i - q_i} \ , \tag{1}$$

where, p_i is the probability of ionization a single electron out of the shell (sub-shell). The emission rate of an ensemble of excited atoms will be obtained by averaging over different configurations of vacancies:

$$\overline{\left(\frac{\Gamma_X (K - Y_i)}{\Gamma_K} \right)} = \sum_{q_i} P_{q_i} \frac{\Gamma_X (K - Y_i; q_i)}{\Gamma_K (q)} \ , \tag{2}$$

where, we noted by $q = (q_i, q_j, ...)$ the ensemble of spectator vacancies in the outer shells Y_i, Y_j, ... Here and in the following, the line above a letter mean averaging over vacancy configurations produced in the collision.

After Scofield [28] and McGuire [29], the radiative $\Gamma_X (K–Y_i; q)$ and non-radiative $\Gamma_A (K–Y_iY_j; q)$ widths are proportional to the number of remaining electrons in the shell (Larkins' scaling rule), i.e.

$$\Gamma_X (K - Y_i; q) = \left(1 - \frac{q_i}{N_i} \right) \Gamma_X (K - Y_i) \ , \tag{3}$$

$$\Gamma_A (K - Y_i Y_j; q) = \left(1 - \frac{q_i}{N_i} \right) \left(1 - \frac{q_j}{N_j} \right) \Gamma_A (K - Y_i Y_j) \ . \tag{4}$$

In the latter expression, for $j = i$ we have $N_j = N_i–1$. The total width will be the sum:

$$\Gamma_K (q) = \Gamma_X (q) + \Gamma_A (q) \ . \tag{5}$$

Averaging, we obtain for the radiation width:

$$\overline{\Gamma_X (K - Y_i; q)} \equiv \Gamma_X (K - Y_i; p) = (1 - p_i) \Gamma_X (K - Y_i) \ , \tag{6}$$

and for the total width:

$$\overline{\Gamma_K (q)} \equiv \Gamma_K (p) = \sum_i (1 - p_i) \Gamma_X (K - Y_i) + \sum_{i \le j} (1 - p_i)(1 - p_j) \Gamma_A (K - Y_i Y_j) \ , \tag{7}$$

the averaged (with a bar) quantities being functions of the ensemble of probabilities $p = (p_i , p_j, ...)$ of ionization of the outer shells Y_i, Y_j,.... In the following, the estimations are calculated in the approximation in which the width of a given configuration $\Gamma_K(q)$ is nearly equal to that of the medium configuration of vacancies, noted as $\Gamma_K(p)$:

$$\Gamma_K(q) = \Gamma_K(p)\left[1 + \frac{\Delta\Gamma_K(q,p)}{\Gamma_K(p)}\right], \quad (8)$$

where, the term $\Delta\Gamma(p,q)/\Gamma_K(p)$ is a small quantity. By expanding to the second order, we find expressions like:

$$\overline{\left(\frac{\Gamma_X(K-Y_i;q)}{\Gamma_K(q)}\right)} = \left(\frac{\Gamma_X(K-Y_i;p)}{\Gamma_K(p)}\right)\left\{1 - \frac{p_i}{N_i}\frac{\Gamma(K-Y_i;p)}{\Gamma_K(p)} + \sum\frac{p_j(1-p_j)}{N_j}\frac{\Gamma^2(K-Y_i;p)}{\Gamma_K^2(p)}\right\}, \quad (9)$$

where

$$\Gamma(K-Y_i;p) = \Gamma_X(K-Y_i) + \sum_{i\le j}(1-p_j)\Gamma_A(K-Y_iY_j) + \sum_{i\ge j}(1-p_j)\Gamma_A(K-Y_jY_i). \quad (10)$$

The energy shift could be calculated in the same way:

$$\Delta E_j = \sum_q P(q)\frac{\Gamma_X(K-Y_i;q)}{\Gamma_K(q)}\Delta E_j(q) \Bigg/ \left[\sum_q P(q)\frac{\Gamma_X(K-Y_i;q)}{\Gamma_K(q)}\right], \quad (11)$$

where, $\Delta E_j(q) = \Sigma\, q_i\, \delta E_{ji}$ and δE_{ji} is the medium energy shift of the transition K-Y_j induced by a spectator vacancy in the shell Y_i. The energy shifts of K_α X-ray transitions due to a single L- or M-vacancy were calculated with the relativistic code of Grant [30].

In the previous relationships, the approximation of an unique ionization probability p_i for the shell Y_i was considered. However, taking into account that the dominant X-ray transitions, de-exciting a K-vacancy are K-$L_{2,3}$ and K-$M_{2,3}$ transitions, the present p_L and p_M estimations should primarily characterize the $L_{2,3}$ and $M_{2,3}$ subshells, respectively.

In the calculations, tabulated radiative [31] and non-radiative [32] widths have been used. We give below some relationships used for the present multiple ionization analysis.

The ratios of K_β / K_α X-ray yields could be expressed like:

$$\left(\frac{\overline{\Gamma}_{K\beta}}{\overline{\Gamma}_K}\right) \Bigg/ \left(\frac{\overline{\Gamma}_{K\alpha}}{\overline{\Gamma}_K}\right) = \left(\frac{\Gamma_{K\beta}}{\Gamma_K}\right) \Bigg/ \left(\frac{\Gamma_{K\alpha}}{\Gamma_K}\right)\frac{1-p_M}{1-p_L}\left[1 + 0.19\frac{p_L - 0.12p_M}{1-0.89(p_L+0.12p_M)}\right], \quad (12)$$

where, the widths $\overline{\Gamma}_K$, $\overline{\Gamma}_{K\alpha,\beta}$ correspond to the multiple ionized atoms produced in the collision and Γ_K, $\Gamma_{K\alpha,\beta}$ for atoms having only one K-shell vacancy.

Modification of the K_α X-ray partial width due to multiple ionization effects could be written as:

$$f_{K\alpha} \equiv \left(\frac{\overline{\Gamma}_{K\alpha}}{\overline{\Gamma}_K}\right) \Big/ \left(\frac{\Gamma_{K\alpha}}{\Gamma_K}\right) = \frac{1-p_L}{1-c_1(p_L+0.2p_M)+c_2(p_L+0.12p_M)^2}, \qquad (13)$$

and, analogous, for K_β X-rays. Here, the quantities $\frac{\Gamma_{K\alpha}}{\Gamma_K} = \omega_K \frac{\Gamma_{K\alpha}}{\Gamma_{KX}}$ (ω_K denoting the K-shell fluorescence yield) are tabulated [30, 33, 34] and the coefficients c_1 and c_2 have values of c_1 = 1.48–1.39 and c_2 = 0.53–0.45 for atomic numbers Z= 26–29.

The energy shifts could be written as:

$$\Delta E_{K\alpha} = AN_L p_L \delta E_{L\alpha} + N_M p_M \delta E_{M\alpha}, \qquad (14)$$

for K_α X-rays and an analogous relation for K_β X-rays. Here $\delta E_{L\alpha}$ and $\delta E_{M\alpha}$ are K_α X-ray energy shifts due to one L-shell or M-shell vacancy, respectively; N_L=8 and N_M are occupancy numbers of L- and M-shell, respectively; A is a constant of the order of 1, which is varying in the range of 1.018–1.005 for Z between 26 and 29.

Correction factors for the K-shell fluorescence yields (ω_K) can be calculated using eq. (13) for K_α X-rays and the analogous equation for K_β X-rays, or the approximate formula of Greenberg et al. [35], which depends only on p_L:

$$f_K \equiv \frac{\overline{\omega}_K}{\omega_K} = \frac{1}{1-\frac{8}{7}p_L(1-\omega_K)}, \qquad (15)$$

where, as before, the line above a letter denotes an average over vacancy configurations produced in the collision. The two mentioned calculation procedures give comparable f_K values.

3. EXPERIMENTAL PROCEDURE

The measurements were performed at the 9 MV Van de Graaff Tandem accelerator of IFIN-HH. The experimental set-up is given in Fig. 1.

Ion beams of $^{16}O^{q+}$ (q = 2–6) enters through a small aperture (2.5 mm diameter) in a vacuum chamber and hits the target placed in the center of the reaction chamber and oriented at 45^0 to the beam direction. We used self-supported thin targets of Ti, Ni, Cu (around 100 μg/cm^2 thickness), Cr and Zr (around 300 μg/cm^2). For X-ray passing, thin Be windows at the scattering chamber and X-ray detectors are provided.

The emitted X-rays were detected using X-ray semiconductor detectors, placed at 90^0 to the beam direction. Namely, we used either an ultra-pure Ge detector in the case of ^{16}O + Cr, Ni, Cu and Zr collisions, with sensitive volume of

100 mm^2 × 10 mm and about 180 eV at 5.9 keV energy resolution, or a Si (Li) detector for the collision of ^{16}O + Ti, having a sensitive volume of 30 mm^2 × 3 mm and an energy resolution of about 200 eV at 5.9 keV. The dead layer of Ge detector was checked by measuring X-ray spectra simultaneously and comparing with the Si(Li) detector.

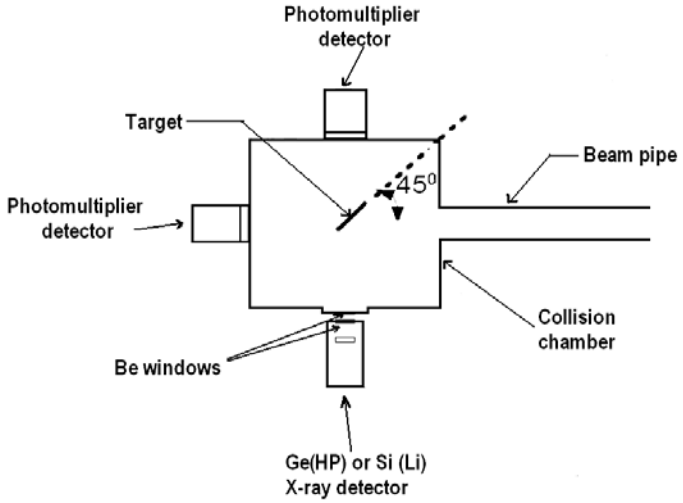

Fig. 1 – Overview of the experimental setup used in the measurements. Using Ge or Si(Li) semiconductor detectors placed at 90^0 to the beam direction, the X-ray spectra have been measured. Scattered ions were detected at either 90^0 or a small angle (about 10.5^0) to the beam direction.

By normalization to the Rutherford scattering cross-sections, X-ray production cross-sections have been determined. The scattered particles were detected with a scintillation detector, consisting of a plastic scintillation foil (of 50 μm thickness) and a photomultiplier. We used two measurement geometries (Fig. 1): for ^{16}O + Ti, Ni, Cu and Zr collisions, a detector placed at 90^0 to the beam direction, while in the case of ^{16}O + Cr collision, a detector placed at a small angle (about 10.5^0) to the beam direction.

The relative efficiencies of the X-ray detectors were obtained using characteristic parameters provided by the producer (Canberra Company, USA) and a model calculation [36]. By measuring standard calibrated ^{241}Am for X-ray (produced by Seibesdorf Laboratory, IAEA) and alpha sources, the solid angles of the X-ray as well as the particle detectors were determined. Worth to mention that for the present used procedure of cross section determination, only the ratio of X-ray and particle solid angles is necessary [see eq. (18) below], which was determined more accurately using the same calibration source (the ^{241}Am alpha source).

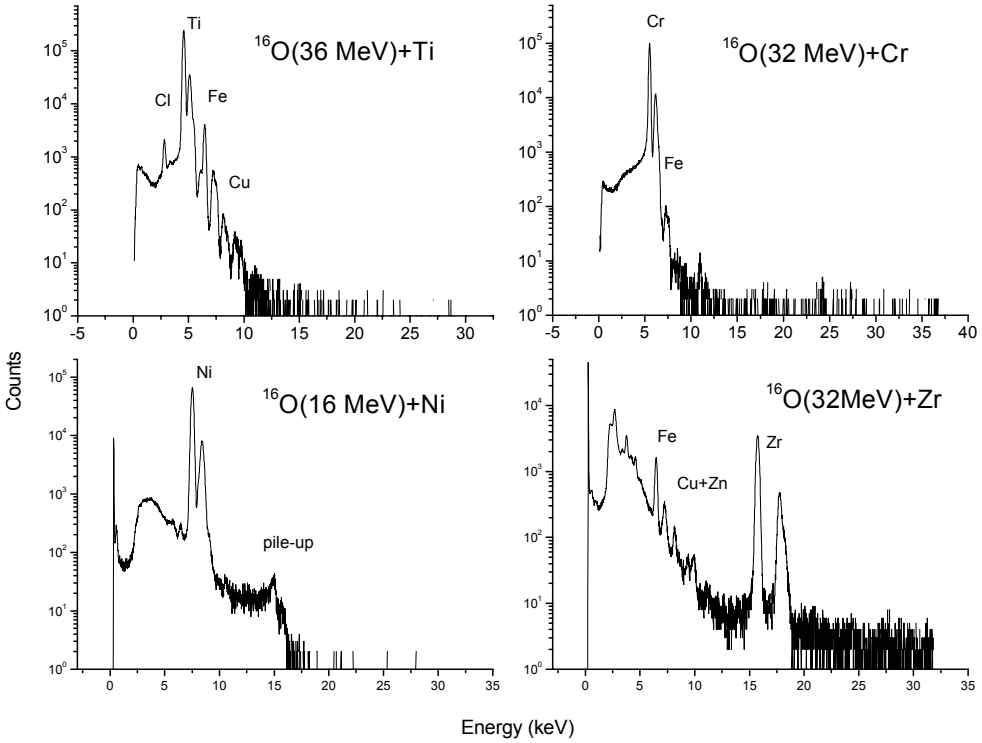

Fig. 2 – Examples of X-ray spectra measured with ^{16}O ions bombarding metal targets at different energies.

The spectra of both X-rays and scattered particles were recorded with a standard spectrometric chain, consisting of linear amplifier, analogue to digital converter (ADC) and a PC based multichannel analyzer. Periodically during the measurements, the energy calibration using X-ray sources (^{55}Fe, ^{57}Co and ^{241}Am) was performed allowing determination of the energy and yield shifts of the K_α and K_β X-ray lines. Using a least squares code (LEONE), with Gaussians fit for X-ray peaks and polynomials of 1-3 degree for the background, the X-ray spectra were processed.

In Fig. 2, examples of X-ray spectra measured with ^{16}O ions bombarding metal targets at different energies are given. In the Figs. 1, 2, in addition to the dominant elements of the target, some of the present impurities are also noted.

In Fig. 3, the X-ray spectrum of a complex thick sample (standard of soil IAEA-SL1), obtained with a beam of ^{16}O at 2 MeV/u energy illustrates both, qualitatively and quantitatively, the applicability of heavier than protons ion beams for elemental analysis.

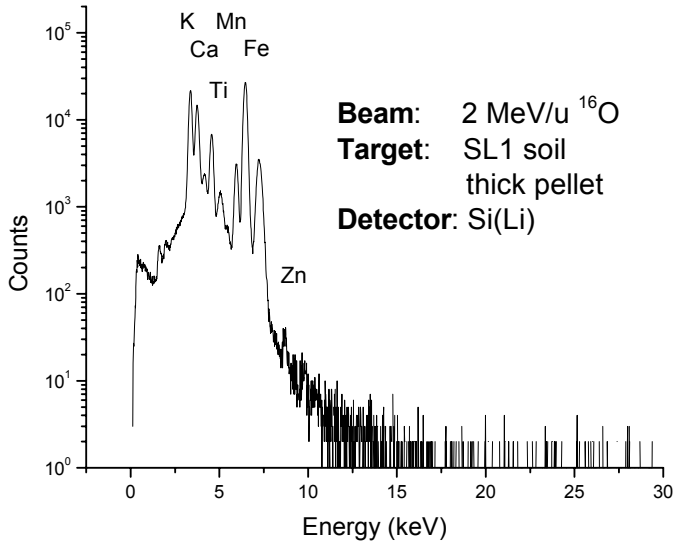

Fig. 3 – The X-ray spectrum of a complex thick sample (standard soil IAEA-SL1) produced by an ^{16}O beam of 32 MeV. The elements whose X-ray lines are visible in the spectrum are marked.

The experimental K-shell ionization cross-sections were determined using the relations written below. The emitted X-ray intensities being proportional to the K-shell ionization cross-sections σ_K, we can write:

$$N_{XK\alpha} \propto \sigma_K \omega_K \frac{\Gamma_{K\alpha}}{\Gamma_{KX}} (\varepsilon f)_{XK\alpha} \left(\frac{d\Omega}{4\pi}\right)_X , \tag{16}$$

where, as before, ω_K is the fluorescence yield, $\frac{\Gamma_{K\alpha}}{\Gamma_{KX}}$ – the branching ratio for the K_α X-ray line, $(\varepsilon f)_{XK\alpha}$ – the relative efficiency for K_α X-rays and $\left(\frac{d\Omega}{4\pi}\right)_X$ – the solid angle of the X-ray detector. For the Rutherford scattered particle intensity we have:

$$N_P \propto d\sigma_R(90^0)\left(\frac{d\Omega}{4\pi}\right)_P , \tag{17}$$

where, $d\sigma_R(90^0)$ is the Rutherford differential cross-section at 90^0 and $\left(\frac{d\Omega}{4\pi}\right)_p$ is the solid angle of the scattered particle detector.

Consequently, the following expression has been used for determination of the K-shell ionization cross-section:

$$\sigma_K = \frac{N_{XK\alpha} \Big/ \left[(\varepsilon f)_{XK\alpha}\, \omega_K \frac{\Gamma_{K,XK\alpha}}{\Gamma_{K,X}} \right]}{N_P} \cdot \frac{\left(\frac{d\Omega}{4\pi}\right)_P}{\left(\frac{d\Omega}{4\pi}\right)_X} \cdot d\sigma_R(90^0). \qquad (18)$$

The statistical and spectra processing uncertainties were < 5% in majority of the cases. The uncertainties due to detector efficiencies are considered to be less than 10% independently of X-ray energy, including the geometric factors (the solid angles) of the X-ray and particle detectors, when the latter is placed at 90^0 to the beam. In case the scattered particles are measured at a forward angle (for Cr target), an additional uncertainty (of 10%) for scattering angle measurement was estimated. We note that using the same (alpha ^{241}Am) source for calibration of both the X-ray and particle detectors, the ratio of their solid angles can be determined more accurately. Therefore, adding quadratically, K X-ray production cross sections uncertainties of 12% for Ti, Ni, Cu, Zr and 15% for Cr (possibly larger due to target thickness correction, especially at the lowest collision energies and at higher target thicknesses) are estimated.

We report polynomial fit values for the quantities characterizing the target multiple ionization: ionization probabilities per electron, p_L and p_M and correction factor f_K for the fluorescence yield. Estimation of their uncertainties is depending on the accuracy of determination of small modifications in the X-ray spectra as well as of model calculations presented in section 2. Taking into account the dispersion of the data for different targets and collision energies, uncertainties of at least 15% for the outer-shell ionization probabilities per electron and 25% for (f_K–1) have been estimated. Therefore, the uncertainties are at least of 14% in case of Ti, Ni, Cu, and Zr and 17% in case of Cr for the present reported K-shell ionization cross sections.

4. RESULTS AND DISCUSSION

Experimental results of multiple ionization analysis as well as of the ionization cross-sections are given.

4.1. MULTIPLE IONIZATION

The relations $p_L \equiv P_L(0) = \frac{1}{8}\bar{n}_L$ and $p_M \equiv P_M(0) = \frac{\bar{n}_M}{N_M}$ were used, where $\bar{n}_L$, $\bar{n}_M$ are the mean numbers of L and M-vacancies, respectively, and N_M is the

occupancy number for the M-shell. This relationships are valid in the independent electron approximation (as the whole calculation presented in section 2), where:

(i) the vacancy states $K_\alpha L^l$ and $K_\alpha M^m$ follows a binomial distribution,

(ii) the variation of fluorescence yield is neglected, and

(iii) the vacancy rearrangements due to non-radiation (Auger and Coster-Kronig) transitions in the outer-shells, prior to the K-shell vacancy de-excitation are neglected.

As shown before by Watson et al. [37], introducing a model which takes into account the rearrangement and fluorescence yield variations does not lead to p_L and p_M probabilities values much different from those obtained if these effects are ignored. Also, the observed dependence on Z_1 is only partially explained by considering these effects. Instead, the observed Z_1 dependence of p_L [37] can be explained by a higher binding energy of L-electrons, for which the procedure of Brandt & Lapicki [10] with an additional correction dependent on collision energy is more suitable.

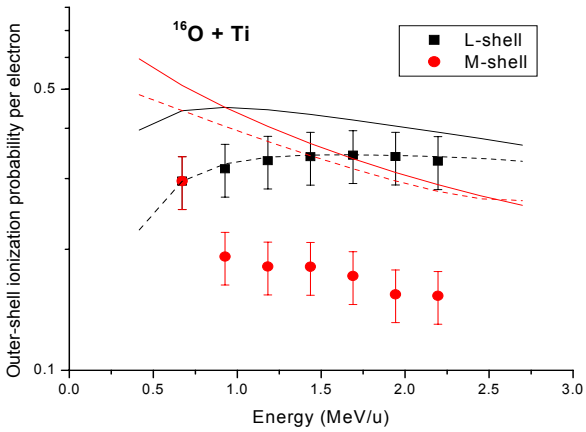

Fig. 4 – Outer- (L- and M-) shell ionization probabilities per electron in the collisions of ^{16}O beams on thin solid Ti target, in dependence on collision energy. The points are the present experimental data obtained using the "yield and energy shifts" method [12] and the lines are predictions of geometrical model [27] calculations, namely solid lines – for tabulated Ti K-shell binding energy [38], dashed lines – for average binding energies corresponding to the final ionization state [39].

Taking into consideration this result, in the present paper we calculate the predictions of the geometric model using enhanced binding energies for L- and M-shells (in all cases, except the case of Zr target). Namely, we used average binding energies of the final state [39], corresponding to the vacancy distributions produced in the L- and M-shells during K-shell ionization collisions; the latter were determined experimentally using "the energy and yield shift method" [12] and IEA calculations. This procedure leads to enhancements of the binding energies comparable to those proposed in ref. [37], where BEA ionization function and BEA scaling after Z_1 were used.

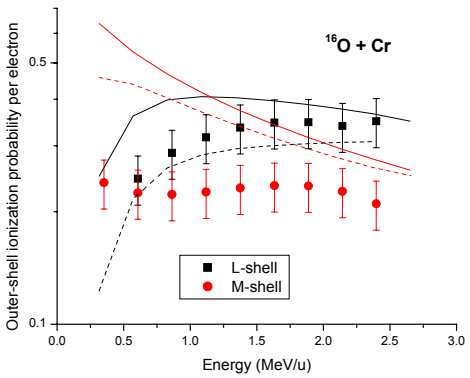

Fig. 5 – The same as Fig. 4, for ^{16}O + Cr collisions.

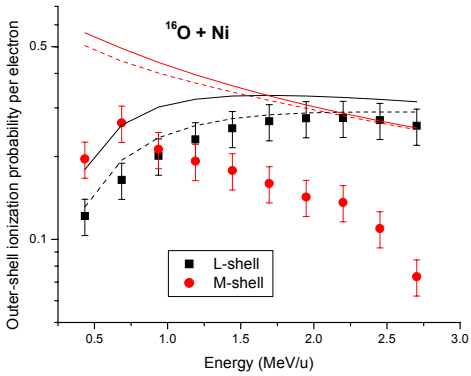

Fig. 6 – The same as Fig. 4, for ^{16}O + Ni collisions.

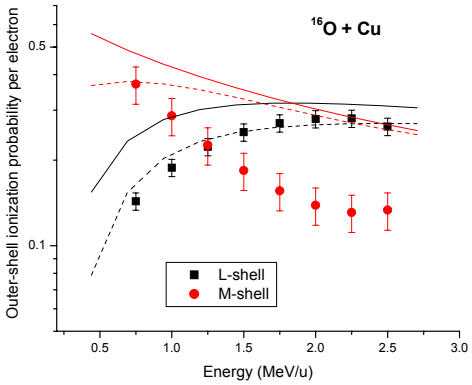

Fig. 7 – The same as Fig. 4, for ^{16}O + Cu collisions.

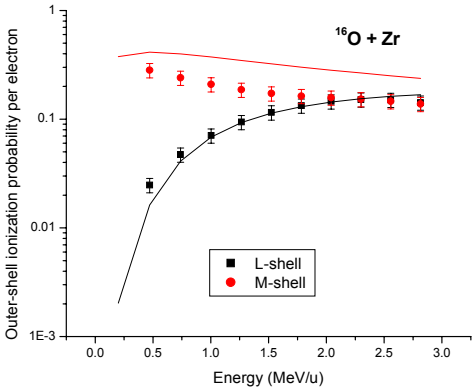

Fig. 8 – The same as Fig. 4, for ^{16}O + Zr collisions.

In Figs. 4–8, the present estimates of L and M outer shell ionization probabilities per electron in the collisions of ^{16}O beams on thin solid targets of Ti, Cr, Ni, Cu and Zr in dependence on collision energy, are given. In the figures the points are the experimental data obtained using the "yield and energy shifts" method [12] (equations (12) and (14) above were used) and the lines are the predictions of the geometrical model [27] calculations, namely: the solid lines, for tabulated K-shell binding energies [38], and dashed lines for average binding energies corresponding to the final ionization state [39].

The multiple ionization probability data are represented in detail in Fig. 9a and 9b for L- and M-shells respectively, in dependence on the parameter X_n of the geometrical model $X_n = 4Z_1V[G(V)]^{1/2} / nv_1$ together with the geometrical model predictions [27]. Here, Z_1 and v_1 are the projectile atomic number and collision velocity, V is the collision v_1 to orbital electron u velocity ratio and n – the

principal quantum number of the outer-shell; $G(V)$ is the BEA model universal function.

As can be seen in the figures, except Zr at the lowest energies in the measured range, the present experimental values of L-shell ionization probabilities per electron are within ±25% compared to geometrical model predictions. Instead, for M-shell ionization probabilities per electron, the geometrical model predictions, corresponding to average binding energies of the final ionization state [39], are higher (in average, by factors of 1.5-2) than the present experimental data.

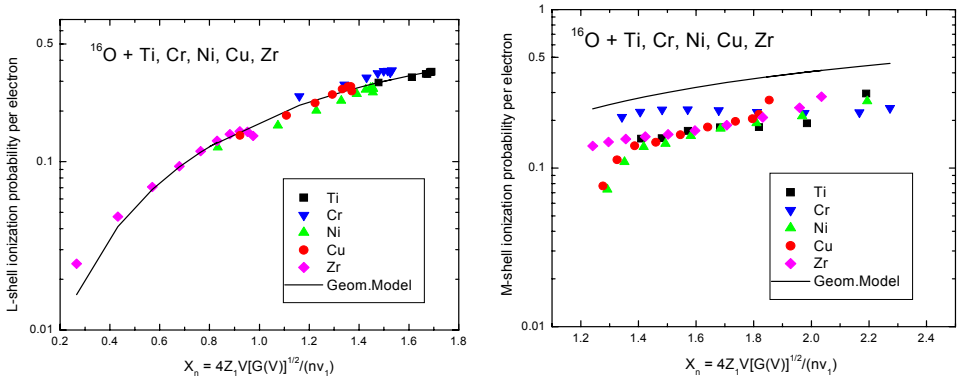

(a) (b)

Fig. 9 – The L- and M- shell ionization probabilities per electron in the collisions of ^{16}O beams on thin solid targets, in dependence on $X_n = 4Z_1V[G(V)]^{1/2}/nv_1$, the parameter of the geometrical model (see text) [27]. The points are the present experimental data obtained using the "yield and energy shifts" method [12] and the line - predictions of the geometrical model.

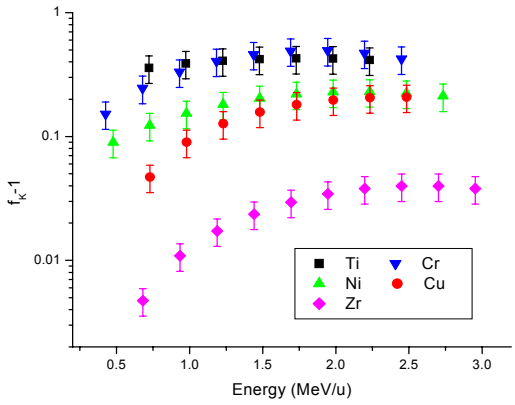

Fig. 10 – Experimental (f_K–1) values, where f_K are correction factors of the K-shell fluorescence yield, obtained in the ^{16}O + Ti, Cr, Ni, Cu, and Zr collisions, in dependence on collision energy. The Greenberg approximate formula [eq. (15)] was used.Values obtained from polynomial fit of the experimental points are represented.

For the correction factors of the fluorescence yields, the Greenberg formula (15) was used. The results obtained for the ^{16}O + Ti, Cr, Ni, Cu, and Zr collisions are given in Fig. 10 in dependence on collision energy. Correction factors for multiple ionization effects as large as 1.5 for Ti and Cr have been obtained. They decrease for higher-Z elements to become ≤ 1.05 in the case of Zr.

4.2. K-SHELL IONIZATION CROSS SECTIONS

In Figs. 11–15, the present experimental values of K-shell ionization cross sections are given and compared with theoretical predictions of the semi-classical approximation (SCA) [9] for two limit cases, the separated atom (SA) approximation, where the binding energy of the target atom with $Z = Z_2$ and united atom (UA) approximation, where the binding energy of the united atom having $Z = Z_1 + Z_2$, are considered, as well as of the ECPSSR model [10].

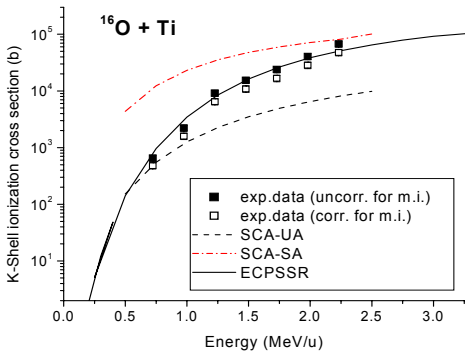

Fig. 11 – Ti K-shell ionization cross sections in the collision with ^{16}O beams in dependence of collision energy. Experimental data, uncorrected and corrected for outer-shell multiple ionization (m.i.) effects, are given. The lines are predictions of theoretical calculations (see text).

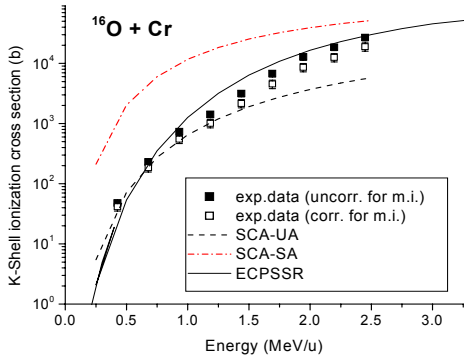

Fig. 12 – The same as Fig. 11, for ^{16}O + Cr collisions.

As expected, the present experimental data, except for Zr, are placed between the two limits of SCA predictions mainly due to the effect of variation of the electron binding energy in the initial state in dependence on the collision velocity (the „binding" effect), while in calculations the electron binding energy is taken constant. For Zr, SCA-UA calculations produce predictions close to the data, although slightly higher.

Instead, the calculation recipes of ECPSSR model, most important those for the binding energy correction, produce theoretical predictions which are in close proximity to the experimental data, although slightly higher in most cases, as seen in the figures.

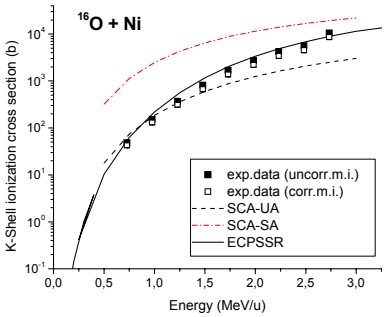

Fig. 13 – The same as Fig. 11, for ^{16}O + Ni collisions.

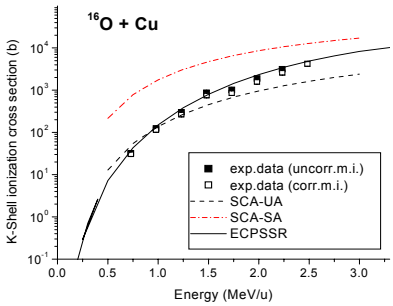

Fig. 14 - The same as Fig. 11 for ^{16}O + Cu collisions.

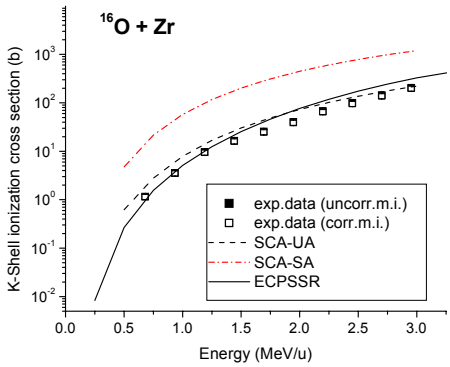

Fig. 15 – The same as Fig. 11 for ^{16}O + Zr collisions.

5. CONCLUSION

In the present paper, K-shell ionization of Ti, Cr, Ni, Cu and Zr in collision with ^{16}O ions, in the energy range of 0,5–3 MeV/u, by measuring the X-ray spectra, has been studied. An analysis of the multiple ionization of the outer (L, M) shells during K-shell ionization, by measuring the energy and yield shifts of the K X-rays [12] was performed. The calculation procedure of multiple ionization effects is presented in some detail in section 2 of the present paper. Outer-shell average numbers of the spectator vacancies, or equivalently ionization probabilities per electron, as well as correction factors to the fluorescence yields due to multiple ionization effects have been estimated. Theoretical predictions of the geometrical model [27], calculated using enhanced (final state) binding energies for L- and M-shells, are within ±25% compared to the experimental values of ionization probabilities per electron for the L-shell, and much higher for the M-shell. Correction factors for multiple ionization effects are as large as 1.5 for Ti and Cr and decrease for Ni and Cu to become less than 1.05 in the case of Zr.

The experimental results for K-shell ionization cross sections were compared with the semi-classical approximation (SCA) calculations [9], in two limits for the electron binding energy in the initial state: the separated atom (SA) and united atom (UA) limits. This comparison highlighted the importance of the "binding" effect. Instead, the ECPSSR [10] model calculations are in close proximity to the experimental data, although slightly higher. The cross section data reported here complete the existing atomic ionization cross section database, which could be of interest for elemental analysis by the PIXE method using heavier ions (^{16}O).

REFERENCES

1. S. A. E. JOHANSSON and T.B. JOHANSSON, Nucl. Instrum. Meth., **137**, 473 (1976).
2. T. DUPUIS et al., Nucl. Instrum. Meth. B, **268**, 1911 (2010).
3. E.A. PREOTEASA et al., X-Ray Spectrom., **38** , 548 (2009).
4. F. FOLKMANN et al., Nucl. Instrum. Meth., **119**, 117 (1974).
5. J.L. CAMPBELL et al., Nucl. Instrum. Meth., **212**, 427 (1983).
6. H. PAUL and J. SACHER, At. Data Nucl. Data Tabl., **42**, 105 (1989).
7 G. LAPICKI, X-Ray Spectrom., **34**, 269 (2005).
8. R. MERZBACHER and H. W. LEWIS, Handb. Phys., **34,** 166 (1958).
9. D. TRAUTMANN and F. RÖSEL, Nucl. Instr. Meth., **169**, 259 (1980).
10. W. BRANDT and G. LAPICKI, Phys. Rev., A. **23**, 1717 (1981).
11. V. HORVAT, Comput. Phys. Comm. **180**, 995 (2009).
12. A. BERINDE et al.,*Atomic and Nuclear Heavy Ion Interactions*, Proc. Int. School on Physics (Brasov, Romania, 1984), eds. A. BERINDE et al., CIP, Bucharest, 1986, Vol. **1**, 453 and 461.
13. T.J. GRAY et al., Phys. Rev. A, **13**, 1344 (1976).
14. B. KNAF et al., Z. Phys. A, **282**, 25 (1977).
15. J. HALL et al., Phys. Rev. A, **28**, 99 (1983).
16. J. SEIDEL et al., Phys. Rev. A, **32**, 2142 (1985).
17. M. GERETSCHLÄGER et al., Phys. Rev. A, **34**, 866 (1986); **45**, 2842 (1992).
18. C. W. WANG et al., Nucl. Instrum. Meth. B, **79**, 190 (1993).
19. B. B. DHAL et al., Phys. Rev. A, **62**, 022714 (2000).
20. P.G. HANSEN et al., in *Atomic Inner Shell Physics*, Ed. B. Crasemann, Plenum, New York, 1975, p. 237.
21. R .L. KAUFMANN et al., Phys. Rev. A, **8**, 1233 (1973).
22. A. R. KNUDSON et al., Phys. Rev. A, **10**, 2118(1979).
23. C. R. VANE et al., Nucl. Instrum. Meth. B, **10/11**, 190 (1985).
24. B. PERNY, et al., Phys. Rev. A, **36**, 2120 (1987).
25. J. M. HANSTEEN and D.P. MOSEBEKK, Phys. Rev. Lett., **29**, 1361 (1972).
26. J. H. McGUIRE and L. WEAVER, Phys. Rev A, **16**, 41 (1977).
27. B. SULIK et al., J. Phys. B **17**, 3239 (1984); Nucl. Instrum. Meth. B, **28**, 509-518 (1987).
28. J.H. SCOFIELD, in *Atomic Inner Shell Physics*, Ed. B. Crasemann, Plenum, New York, 1975, p. 265.
29. E. J. McGUIRE, in *Atomic Inner Shell Physic*s, Ed. B. Crasemann, Plenum, New York, 1975, p. 293.
30. I. P. GRANT et al., Comput. Phys. Comm., **21**, 207 (1980).

31. J. H. SCOFIELD, At. Data Nucl. Data Tabl., **14**, 121 (1974).
32. M. H. CHEN et al., At. Data Nucl. Data Tabl., **24**, 13 (1979).
33. M.O. KRAUSE, J. Phys. Chem. Ref. Data, **8**, 307 (1979).
34. S. I. SALEM et al., At. Data Nucl. Data Tabl., **14**, 91 (1974).
35. J. S. GREENBERG et al., Phys. Rev. A, **16,** 964 (1977).
36. J. S. HANSEN et al., Nucl. Instrum. Meth., **106**, 365 (1973).
37. R. L. WATSON et al., Phys. Rev. A, **19**, 1529 (1979).
38. J. A. BEARDEN and A.F. BURR, Rev. Mod. Phys., **39**, 125 (1967).
39. W. LOTZ, J. Opt. Soc. Am., **58**, 915-921 (1968).